Journal of Biomechanics 44 (2011) 2409–2417

Contents lists available at ScienceDirect

Journal of Biomechanics

journal homepage: www.elsevier.com/locate/jbiomech
www.JBiomech.com

Fluid–structure interaction study of the edge-to-edge repair technique on the mitral valve

K.D. Lau [a,c,*], V. Díaz-Zuccarini [c], P. Scambler [b], G. Burriesci [c]

[a] Centre for Mathematics and Physics in the Life Sciences and Experimental Biology (CoMPLEX), UCL, United Kingdom
[b] UCL Institute of Child Health, United Kingdom
[c] Department of Mechanical Engineering, UCL, United Kingdom

ARTICLE INFO

Article history:
Accepted 26 June 2010

Keywords:
Valve repair
Edge-to-edge
Mitral valve
Finite element
Fluid–structure interaction

ABSTRACT

The effect of functional mitral regurgitation has been investigated in an anatomically sized, fluid–structure interaction mitral valve model, where simulated correction has been performed by applying: (1) edge-to-edge repair with annuloplasty and (2) edge-to-edge repair only. Initially defined in an open unstressed/corrected configuration, fluid–structure interaction simulations of diastole have been performed in a rigid ventricular volume. Comparison of the maximum principal stresses (during diastole) in the normal and repaired models has shown that the magnitude of stress in the repaired scenarios is ~200% greater. The combined edge-to-edge and annuloplasty procedure was found to spread the induced stresses across the free margin of the leaflets, whereas without annuloplasty a localised stress concentration in the region of the suture was observed. Fluid flow downstream of the corrected configurations was able to achieve the same magnitude as in the normal case, although the flow rate was impaired. The maximum flow rate was found to be reduced by 44–50% with the peak flow rate shifted from the end of the diastole in the normal case to the start in the repaired cases.

1. Introduction

The most common dysfunction of the mitral valve (MV) is mitral valve regurgitation (MVR) which accounts for ~70% of native MV dysfunctions (Iung et al., 2003). In MVR abnormal amounts of retrograde flow enter the atrial chamber increasing the haemodynamic load in the left heart, a factor which can lead to cardiac related pathologies such as ventricular and atrial dilation, hypertrophy and atrial fibrillation (Verma and Mesana, 2009). The etiologies of MVR can be divided between structural (primary) and functional (secondary) dysfunctions. Structural dysfunctions are caused by factors which affect the tissue of the valve, resulting in a loss of biomechanical strength (i.e. myxomatous mitral tissue degeneration). Functional dysfunctions result from indirect factors which do not affect the tissue, but impact the function of the valvular subcomponents (i.e. annular dilation or papillary muscle displacement) (Alfieri and Bonis, 2010). Correction of regurgitation is performed by repairing existing valve anatomy or replacement by prosthetic substitute. Repair is preferred if possible as mortality rates are reduced (2.0% against 6.1% for replacement) and other related complications such as thromboses are minimised (Anyanwu et al., 2010).

1.1. Mitral valve repair

Using the existing anatomy, MV repair attempts to improve compromised valvular function. The most common approach is annuloplasty, in which a prosthetic ring is implanted to reshape the annulus geometry to a functional state. A range of different options exist which include rigid/semi-rigid or flexible devices, with closed or partial ring designs.

Another repair method is the edge-to-edge repair (ETER) technique designed by Alfieri (see Alfieri and Bonis, 2010). This technique rectifies prolapse through restoring coaptation by joining the prolapsing segment(s) to the opposing leaflets. By repairing the existing valve structure the ETER reduces the severity of the regurgitation during systole, improving factors such as the ejection fraction (Kinnaird et al., 2003). However, the ETER reduces both the geometric and effective orifice areas of the valve during diastole, altering the normal stress state of the valve and fluid dynamics during diastolic filling.

Traditionally the ETER is performed via a midline sternotomy and in conjunction with annuloplasty, a factor which has had positive clinical results in particular when annular function is compromised (Alfieri and Bonis, 2010; Maisano et al., 2003). Recently less invasive approaches have been pioneered whereby the ETER repair is performed using a clip, rather than sutures. Delivered via percutaneous access through the femoral venous transseptal path, this clip consists of two metallic arms which grip and hold the prolapsing segments of the leaflets together as the

* Corresponding author at: Centre for Mathematics and Physics in the Life Sciences and Experimental Biology (CoMPLEX), UCL, Physics Building, Gower Street, London, WC1E 6BT, United Kingdom.
E-mail address: k.lau@ucl.ac.uk (K.D. Lau).

0021-9290/$ - see front matter © 2011 Elsevier Ltd. All rights reserved.
doi:10.1016/j.jbiomech.2011.06.030

heart beats (Feldman et al., 2009). Less invasive as open access to the heart is no longer required, these methods do not allow the ETER to be supplemented with an annuloplasty ring.

1.2. Finite element models

Although imaging techniques allow non-invasive measurement and visualisation of valve deformation and haemodynamic parameters in normal and diseased states (Veronesi et al., 2009), they cannot provide functional information on the stress state of the valve. In order to extract information on biomechanical function, the support of numerical simulations is essential. The application of numerical methods to heart valves is complicated by the nature of the problem, as throughout the cardiac cycle the heart valves are immersed in blood and subjected to non-uniform haemodynamics loads. Modelling of this problem requires an approach that is able to handle both the large deformation of a non-linear elastic structure and the coupling of fluid and structural domains.

Various models have been reported in the literature and can be broadly divided into structural-only, fluid–structure interaction (FSI) and fluid-only models. Although structural and FSI models of the native MV exist (Votta et al., 2008; Kunzelman et al., 2007), the ETER has been previously modelled using structural-only (Avanzini, 2008; Dal Pan et al., 2005; Votta et al., 2002) or valveless fluid-only approaches (Redaelli et al., 2001), both of which have limitations. Structural-only models assume the haemodynamic pressure load is uniform over the surface of the valve, a factor which has been previously shown to affect valve dynamics (Lau et al., 2010). Fluid-only models yield the non-uniform pressure field across the valve, yet do not account for the deformation of the valve which in turn regulates the flow through the orifice; only with FSI are both of these factors addressed.

Structural-only simulations of the ETER have examined the increase in stresses during diastole and the dual effect of stitch location and length. Votta et al. (2002) report that during diastole a repaired valve experiences principal stresses comparable to that of systole, whereas Dal Pan et al. (2005) and Avanzini (2008) have shown that the lateral positioning and length of the suture both have a positive effect in reducing the magnitude of stress induced; both models also show that the uncorrected dilation of the annulus in a simulated dysfunctional state result in a higher value of stress during diastole.

Fluid-only models (Redaelli et al., 2001) have studied the effect of the ETER by defining a fluid volume with single/double orifice/s representing the corrected valve geometry following ETER. The effects of a single orifice (uncorrected), double orifice (central leaflet correction) and an asymmetric single orifice (commissural leaflet correction) have been examined, with results indicating that the key factor affecting the transvalvular pressure drop is the total cross-sectional area of the repaired valve.

This study presents for the first time, FSI models of the ETER. Using non-linear material models to represent the MV, simulation of the coupled function of the valve and blood has been performed in normal and dysfunctional states representative of functional MVR. Repair has been performed with two different approaches and the resulting variation in stress states and fluid dynamics has been analysed and compared to the uncorrected valve.

2. Methods

The model described here was implemented in the explicit finite element code LS-DYNA (Hallquist, 2006; LS-DYNA Keyword User's Manual, 2007), as it provides the facilities to model both the large deformations of the valve structure and the FSI of the blood with the valve. All simulations and post-processing were performed on a Intel Xeon 2.66 GHz workstation with LS-DYNA 971 Release 4.2.1, LS-PREPOST 3.1, EnSight 9.1.2 and MATLAB R2010b.

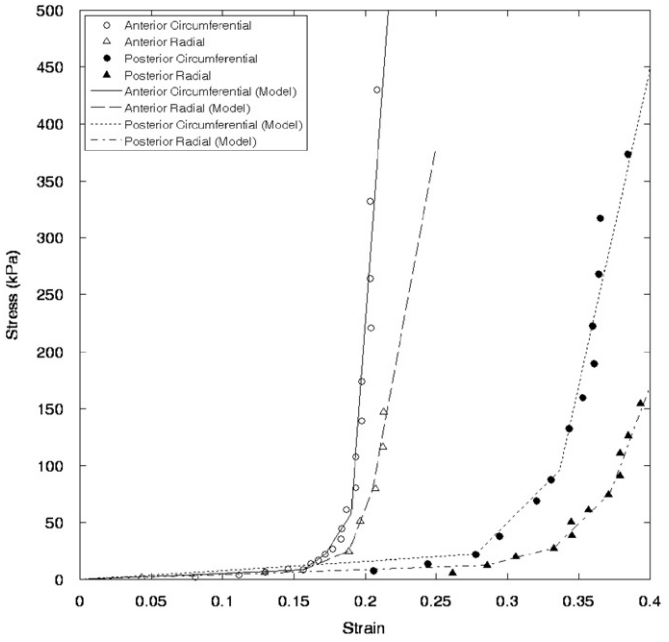

Fig. 1. Stress–strain curves used in the material model of the valve leaflets, digitised experimental data taken from May-Newman and Yin (1995).

2.1. Normal and dysfunctional states

Valve function has been examined in normal and dysfunctional states, repaired with the ETER, with/without annuloplasty. Functional MVR has been simulated by dilating the annulus and assuming the biomechanical properties of both the leaflets and chordae remain same between the normal and dysfunctional states, a factor traditionally reflective of functional MVR.

In vivo echocardiographic comparison of human patients with both normal and regurgitant MV function has shown that the annulus of the valve is more dilated in this dysfunctional state. Under normal conditions the annulus is a highly dynamic structure, varying in eccentricity[1] from 0.57 at mid-systole to 0.42 in mid-diastole. In dysfunctional states the annulus of the valve is less dynamic, varying from 0.50 in mid-systole to 0.42 in mid-diastole (Kaplan et al., 2000).

Using this data (Kaplan et al., 2000), a dysfunctional state was modelled by dilation of the valvular orifice in the anteropostero axis. Following this, correction was simulated in two separate scenarios in order to examine the difference between traditional and endovascular techniques for the ETER. Comparison of these states was performed against an undilated and uncorrected model, which is referred to as the normal state.

2.2. Material model

The biomechanical response of the leaflets has been defined using the biaxial stress–strain experiments performed by May-Newman and Yin (1995), the reported stress–strain curves have been discretised by selecting key data points as shown in Fig. 1 and input into the material model `MAT_NONLINEAR_ORTHOTROPIC` in LS-DYNA (LS-DYNA Keyword User's Manual, 2007). As the MV leaflets are modelled as membranes, reduced integration across the shell thickness was performed. For further details regarding this material model, refer to Appendix A.1 (Kunzelman et al., 1993; Benson, 1992; Batchelor, 1967).

The chordae are modelled as beams which generates force solely under tension. The non-linear mechanical properties of the chordae are defined from experimental data (Kunzelman and Cochran, 1990) and were input into the material model `MAT_CABLE_DISCRETE_BEAM` (LS-DYNA Keyword User's Manual, 2007).

2.3. Mitral valve model

The MV geometry is based upon anatomical measurements reported from *in*/*ex vivo* sources. The valve has been modelled as symmetric about the anteropostero axis, allowing the computational simplification of only simulating half the MV. The density (ρ) of all valvular parts has been taken as 1 g cm^{-3}.

[1] Eccentricity (e) is defined as $e=\sqrt{a^2+b^2}/a$, where a and b are the major and minor axes of the orifice.

The base of the model, the normal (undilated) annulus was defined as a static and planar D-shaped orifice with an anteropostero and commissural diameters of 22.5 and 30 mm, respectively (Fig. 2). Using the centre of the anterior leaflet as a reference point, the annular extent of the valvular cusps was defined by scaling reported data (Sakai et al., 1999) to the D-shaped orifice. The perimeter of the annulus and its enclosed area in the normal state are 8.67 cm and 5.54 cm^2, respectively.

Extending from the annulus are the cusps of the leaflets, represented here by the larger anterior and three smaller posterior cusps (Fig. 2). Sized from anatomical measurements (Kunzelman et al., 1994), the areas formed by the leaflets have been meshed using rectangular shell elements. Measurements of the leaflet thickness show regional differences between leaflets (May-Newman and Yin, 1995), however, no detailed description of this variation exists in the literature. This variation in thickness has been simplified by modelled both leaflets as uniformly equal to 1 mm. In total the mesh consisted of 4000 Belytschko-Lin-Tsay shell elements, the resolution was determined to be sufficient by performing a mesh independence analysis. For further details regarding the shell element used, refer to Appendix A.2.

During valve closure inversion of the valve is prevented by the chordae tendineae (CT), structures which are classified by the anatomical position where they attach to the leaflet. Here only the marginal and basal CT have been included, which respectively support the free edges of the leaflets and the base of the valve near the annulus. Anatomical observations indicate that the number and distribution of CT vary significantly, for example the number of marginal chordae attached to the anterior leaflet can range from 5 to 13 (Lam et al., 1970). In this model, the CT distribution was modified to achieve physiological coaptation under closure conditions. In total, the CT consist of 1666 discrete beam/cable elements. The cross-sectional area of the marginal and basal chordae has been taken as 0.45 and 1.15 mm^2, respectively, as reported in Kunzelman et al. (2007).

2.4. Dysfunctional model

Here a state of functional MVR has been modelled where dysfunction is generated from a change in annular dimension, whilst the function of the leaflets and chordae has been assumed to remain normal. Utilising the same material model described previously, the MV model was dilated in the anteropostero axis by a factor of 1.11 decreasing the eccentricity from 0.66 to 0.56, consistent with the average reduction in eccentricity of 15.5% during diastole as reported by Kaplan et al. (2000) (see Fig. 2). This dilation increased the leaflet surface area by 3.7%, annulus length to 8.96 cm and MV orifice area to 6.04 cm^2. This modified geometry is the reference geometry for the dysfunctional state and was defined as stress-free.

The ETER was simulated by first connecting the central region of the free margin, over a width of 2 mm on both anterior and posterior leaflets, with thermal beam elements. Following this, application of a negative thermal load (a linear ramp of -5 °C over 100 ms) was used to contract these beams, connecting the two edges together completing the simulation of the ETER (Fig. 2). This single Hughes–Liu beam was defined with a density of 1 g cm^{-3}, an elastic modulus of 1 MPa and a thermal coefficient of expansion 1 $°C^{-1}$. The values of these parameters were set to reduce the length of the beam connecting both leaflet edges by $\sim 99\%$, ensuring the connection of the two leaflet portions.

2.5. Valve repair

The ETER was examined using two different approaches: the standard surgical approach with supplementary annuloplasty and the endovascular approach that

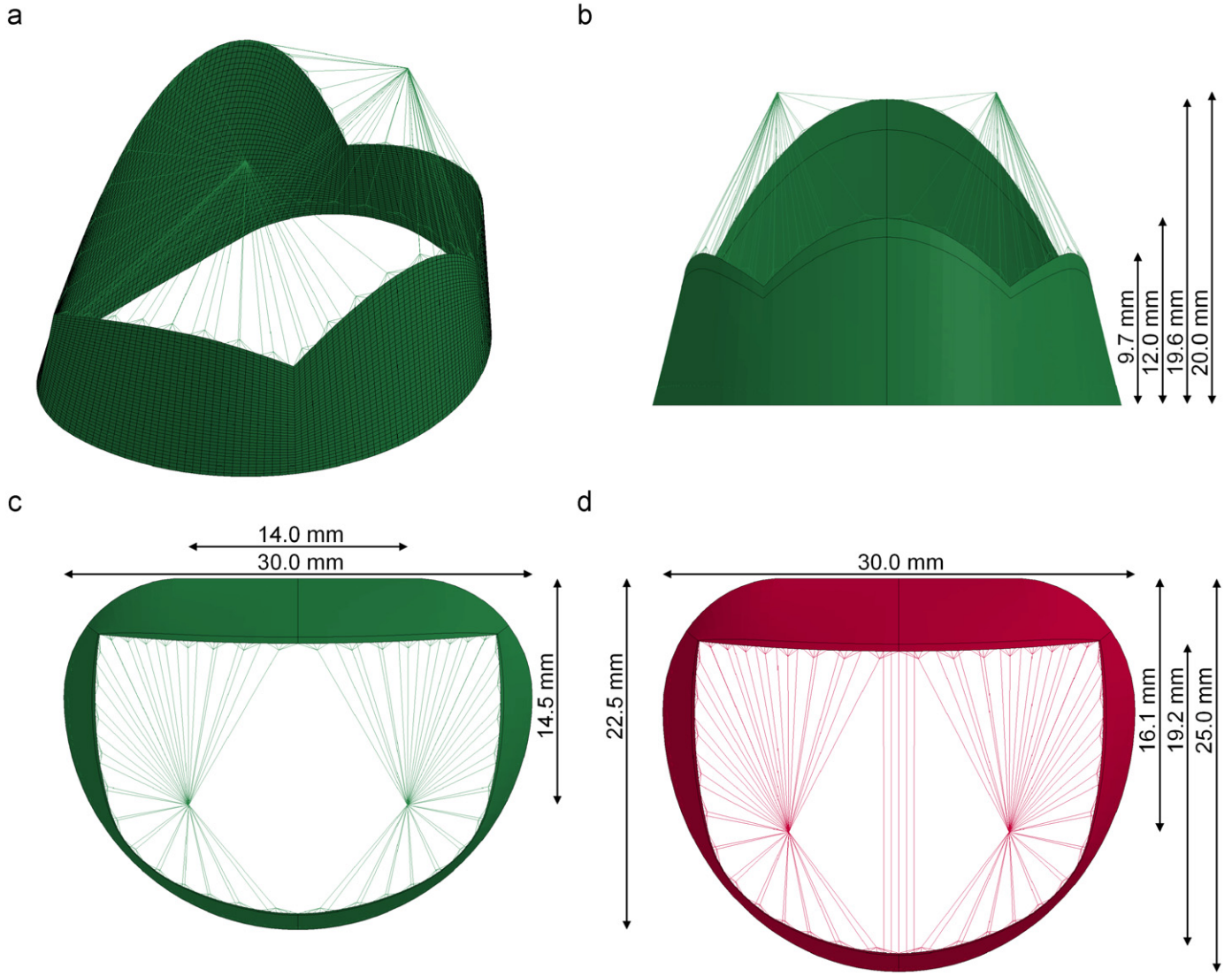

Fig. 2. Finite element model of the MV: (a) 3D view with finite element mesh superimposed, (b) front view, (c) top down view (normal) and (d) top down view (dysfunctional). All units in mm.

allows only the ETER (Fig. 3). Both cases are first defined in a dysfunctional state through valvular dilation. In the case of simultaneous ETER and annuloplasty, the nodes of the annulus are also displaced back to the D-shape of the normal annulus, mimicking the effect of a rigid annuloplasty ring. For the ETER-only case, only the thermal beams are contracted and the annulus remains dilated.

Contraction of the beam elements was performed with structural-only simulations for computational efficiency. The dampening effect of the fluid was approximated by using a global nodal damping factor of 0.9965, based on previous experimental results (Burriesci et al., 1999). The final configuration (geometry and stress state) was used as the initial state for the corresponding FSI simulations, prior to which the thermal beam elements were switched from deformable to rigid objects.

2.6. Fluid–structure interaction model

FSI was performed by immersing the valve model into an overlapping U-shaped fluid domain, volumetrically sized with left ventricular and atrial volumes of 85 and 35 ml, respectively (Fig. 4) (Levick, 2003). Although the ventricle has been defined using an un-physiologically rigid volume, previous FSI analysis has shown that differences in valvular dynamics exists between straight and more physiological U-shaped geometries (Lau et al., 2010). Using a structured mesh, the volume was designed to include the shape of the mitral and aortic orifices (Fig. 4). The final meshed geometry of the fluid volume with the normal annulus consisted of 20430 LS-DYNA 8-node brick elements. In the dilated geometry the larger orifice increased the number of fluid elements, resulting in a fluid volume with 30,618 elements. Parameters have been chosen to reflect the higher density and dynamic viscosity of blood, which has been modelled as a Newtonian fluid (Table 1). Mesh independence was verified on a series of fluid-only analyses by applying the pressure boundary condition of the full simulation up to maximum value of pressure (Fig. 5). Coupling of the fluid/structure was performed using a

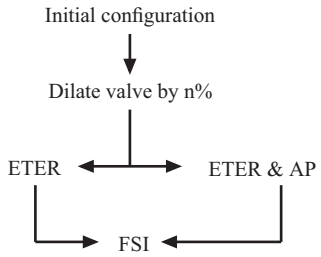

Fig. 3. Valve correction simulation flow.

Table 1
Fluid properties.

Parameter	Value
Density (ρ)	1.080 g cm^{-3}
Dynamic viscosity (v)	0.0039 Pa s
Bulk modulus (K)	22 GPa

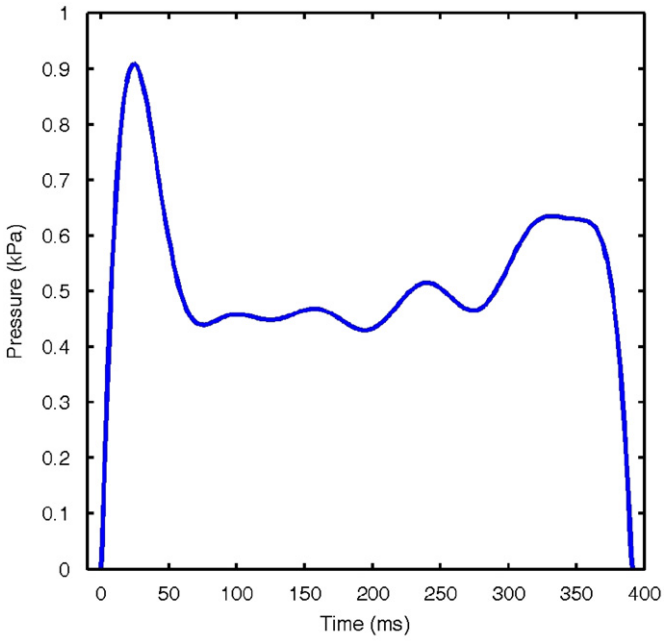

Fig. 5. Transvalvular pressure difference between left atrium and ventricle during diastole. The zero pressure difference marks the pressure cross-over points in the cardiac cycle, indicating the start and end of diastole. Average transvalvular pressure was 0.52 kPa (3.9 mmHg). Data after Levick (2003).

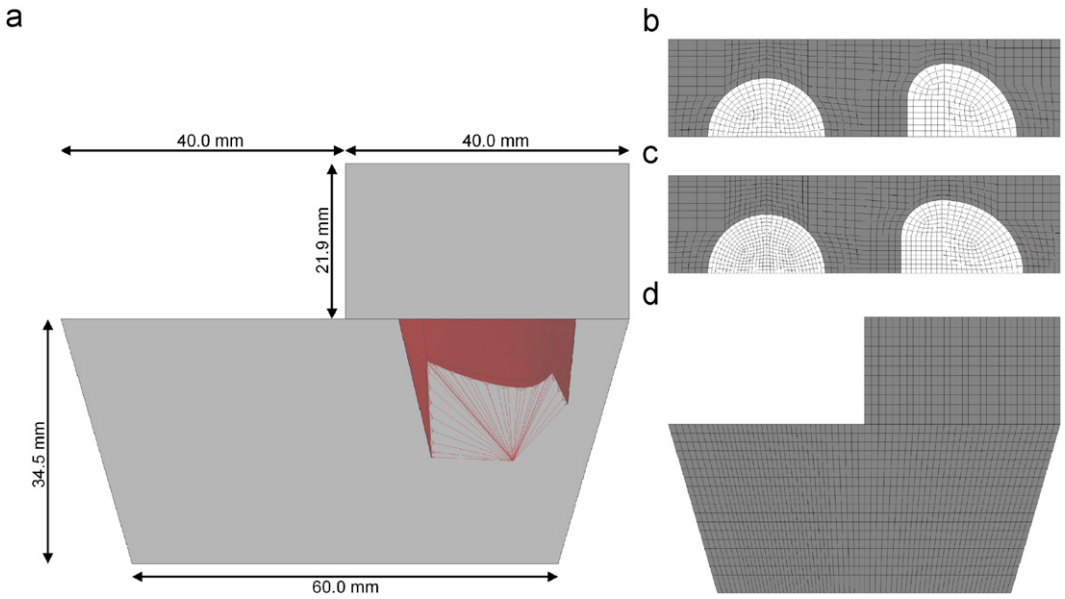

Fig. 4. (a) Fluid volume geometry in which the MV model is immersed into (highlighted in red), (b) top down view of the normal mesh with the valvular orifices highlighted in white, (c) top down view of the dilated mitral annulus model and (d) side view of the normal fluid volume mesh. The volume of the atrial and ventricular chambers were sized to 35 and 85 ml, respectively. (For interpretation of the references to color in this figure legend, the reader is referred to the web version of this article.)

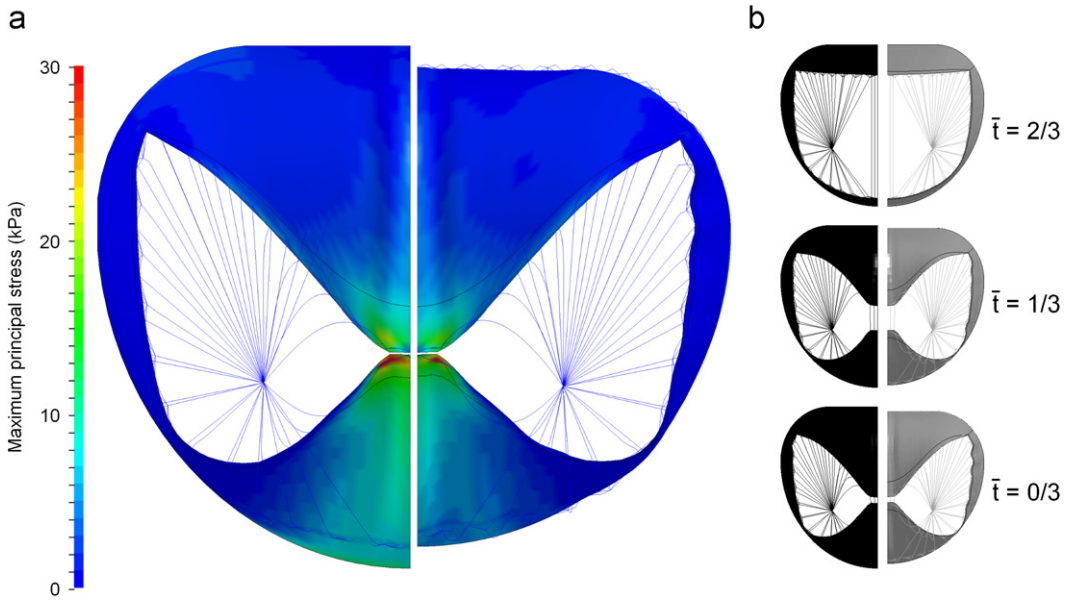

Fig. 6. Simulation of the ETER correction in the dilated MV model; (a) maximum principal stress distribution in its final state, $\bar{t} = t/t_{max} = 1$, without (left) and with (right) annuloplasty; (b) the corresponding deformation at $\bar{t} = t/t_{max} = 0/3$, 1/3 and 2/3, without (left) and with (right) annuloplasty.

penalty coupling method. For further details regarding this and other aspects of the fluid–structure interaction model, refer to Appendix A.3.

2.7. Boundary conditions

Previous transient FSI simulations of a single cardiac cycle ($\sim$1000 ms) with the available computer equipment have required approximately 100 h of computer time (Lau et al., 2010). Here the focus is in the diastolic component of the cardiac cycle, thus these simulations have been limited to that portion only. Starting with the valve in an open configuration, the ETER was first performed (in dysfunctional states) and immediately followed by the application of a diastolic pressure gradient simulating fluid flow through the valve (Fig. 5). The pressure curve used in these models was described using a 6th order Fourier series[2] (Eq. (1)) where the units of pressure and time are mmHg and ms, respectively:

$$\Delta P(t) = a_0 + \sum_{n=1}^{6} a_n \cos(nwt) + \sum_{n=1}^{6} b_n \sin(nwt) \quad (1)$$

3. Results

3.1. Valve correction

ETER has been simulated by central correction of the anterior and posterior leaflets with and without annular displacement. The deformation of the valve and the maximum of the principal stresses from this deformation are shown in Fig. 6.

3.2. Valve dynamics

The values of the maximum principal stresses induced in the normal and two dysfunctional models are listed in Table 2. The deformation and stress distribution in each model at its maximum principal stress is visualised in Fig. 7.

[2] Fourier coefficients: $a_0 = -6.299$, $a_1 = -13.21$, $a_2 = 0.7083$, $a_3 = 8.703$, $a_4 = 7.035$, $a_5 = 2.608$, $a_6 = 0.2057$, $b_1 = 13.55$, $b_2 = 16.41$, $b_3 = 8.148$, $b_4 = 0.2259$, $b_5 = -1.848$, $b_6 = -1.006$ and $w = 0.01185$.

Table 2
Maximum principal stress in normal and repaired models.

Model	Max. principal stress (kPa)
Normal	69.7
ETER and AP	195.8
ETER only	205.5

3.3. Fluid dynamics

The ETER reduces the flow rate through the orifice throughout the diastolic cycle in both corrected configurations (Fig. 8). Comparison of the velocity magnitude downstream of the MV is visualised using the plane located in the centre of the valve, parallel to the anteropostero axis (Fig. 9). Fluid motion through the orifice was also analysed with particle tracing (Fig. 10).

4. Discussion

4.1. Valve dynamics

During diastole the stresses in the uncorrected valve are small, however, the effect of the ETER increases the maximum principal stress by $\sim$200% (Table 2). The maximum diastolic principal stresses in the repaired valves equate to 65% (ETER with annuloplasty) and 68% (ETER only) of the maximum principal stress observed in the same model during systolic closure only ($\sim$300 kPa). Using a linear elastic orthotropic model, Votta et al. (2002) performed simulations of the ETER, showing the maximum diastolic stress in a repaired state is comparable to the maximum systolic stress. Similar analysis by Dal Pan et al. (2005) reports the maximum diastolic stress as 71% of the systolic stress. The inconsistencies of these values can be attributed to the fact that structural models are not adequate to model diastole which is a transient event, where the valve is in dynamic motion and the pressure load is non-uniform over the MV surface.

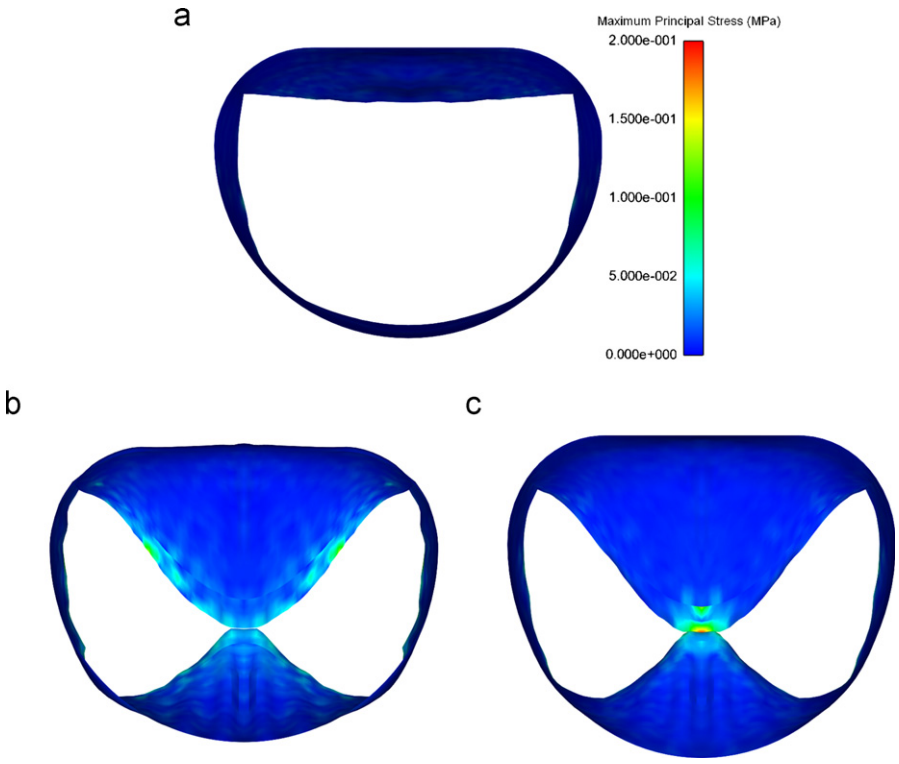

Fig. 7. Valve deformation and maximum principal stress distribution at the local maximum of the principal stress in each model as viewed from the ventricular side of the valve in the (a) normal valve (t=42 ms), (b) ETER valve subjected to annuloplasty (t=340 ms) and (c) ETER only repaired valve (t=101 ms).

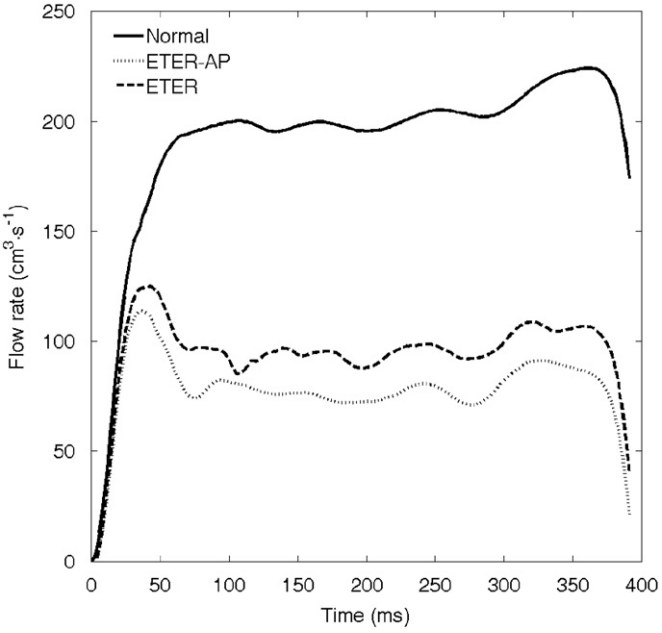

Fig. 8. Flow rate through mitral orifice in the normal valve, ETER with annuloplasty valve and ETER only valve.

Although the magnitude of stresses is similar in both ETER cases, the distribution of stress differs. Comparison of stress at the local maximum of each model shows that with the ETER-only repair a concentrated stress distribution is located at the suture, compared to the ETER with annuloplasty case where the stresses are redistributed along the free margin of leaflets (Fig. 7). This reduction in stress between corrected and uncorrected annular dilation has been also highlighted in previous ETER simulations (Votta et al., 2002; Dal Pan et al., 2005).

Clinical results have shown that the repair of the valve without the application of an annuloplasty ring has suboptimal performance (Alfieri and Bonis, 2010). Although the etiologies of heart valve disease are numerous, it has been possible to explore in detail the effect of one factor here in this model: annular dilation. In this case it has been shown that valve correction without the application of annuloplasty induces a higher maximum stress and a more concentrated stress pattern. This has particular impact upon percutaneous techniques whereby the ETER is the only repair.

4.2. Fluid dynamics

Comparison of the flow rate shows that the ETER impairs the MV's ability to facilitate rapid fluid transport (Fig. 8). The initial flow rate between the normal and repaired valves is comparative over the initial 20 ms of the diastolic simulations. Beyond this point, the difference in magnitude rises to over 100 $cm^3\ s^{-1}$ as the repaired valves are unable to deform freely and increase the flow rate. This is highlighted by the location of the maximum flow rate (Fig. 8) which occurs at $\sim$360 ms in the normal model (13.4 $l\ min^{-1}$) and $\sim$40 ms in the two repaired valves (7.5 and 6.8 $l\ min^{-1}$ for the ETER only and the ETER with annuloplasty) (Table 3).

Downstream of the valve, the maximum magnitude of the fluid velocity is similar in all three models (Fig. 9). Approximately 0.8 m s^{-1}, this value corresponds to expected physiological values (Lau et al., 2010). Particle traces at the maximum velocity point in the cycle highlight that the fluid field in the corrected cases contains large areas of rotation (Fig. 10).

4.3. Limitations

This study only analyses the effect of a centrally located suture, lateral suture positions have not been examined. However, the

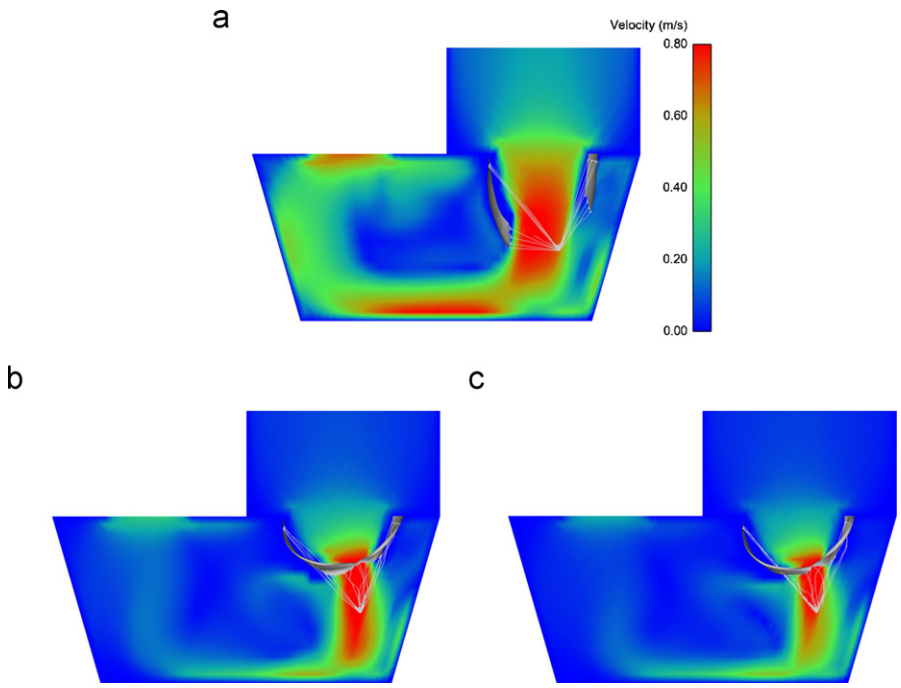

Fig. 9. Fluid velocity distribution through a plane centred in the valve model in the (a) normal valve, (b) ETER and AP corrected valve and (c) ETER only valve. All figures visualised at $t=365$ ms, the point at which the global maximum fluid velocity was observed.

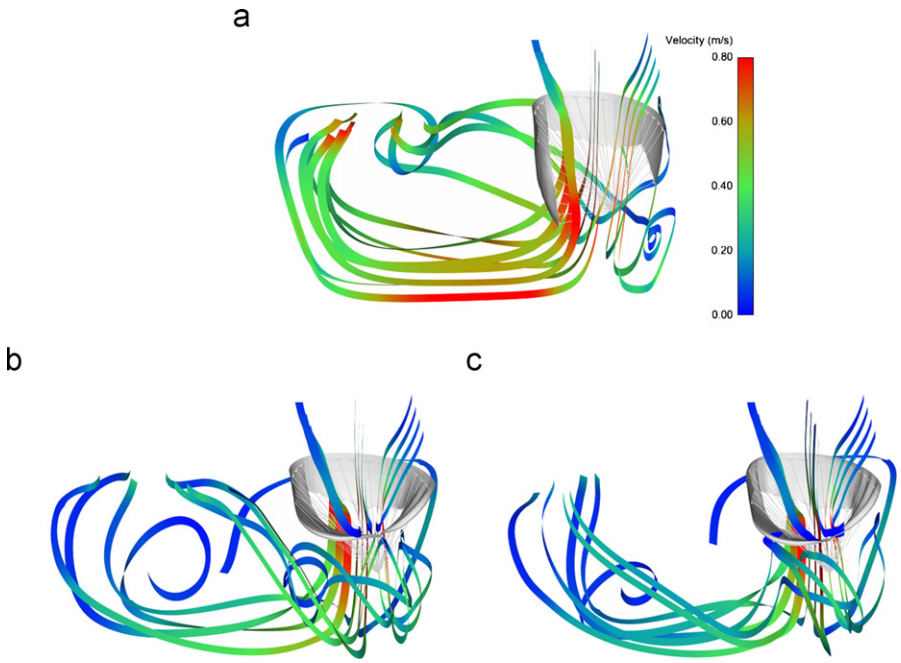

Fig. 10. Particle traces of the fluid field taken at $t=365$ ms. Particles were seeded from a plane located 10 mm above the valve orifice in the (a) normal valve, (b) ETER valve with annuloplasty and (c) ETER only valve.

Table 3
Maximum value of the flow rates in the normal, ETER valve subjected to annuloplasty and ETER only valve.

Model	Flow rate ($cm^3\ s^{-1}$)	Flow rate ($l\ min^{-1}$)
Normal	224	13.4
ETER and AP	114	6.8
ETER only	125	7.5

central suture corresponds to the most severe scenario in terms of the leaflet stress distribution as reported in previous structural analyses of the ETER technique (Avanzini, 2008; Dal Pan et al., 2005; Votta et al., 2002).

The annulus of the valve was modelled as a static planar object, neglecting its dynamic motion, which adopts a 'saddle' shape in the systolic phase (Veronesi et al., 2009). This has been shown to reduce stress concentrations during valve closure (Salgo et al., 2002).

However, the focus of this study was the diastolic peak where the role of the annulus dynamics in the reduction of stress is reduced.

As the valve was defined in its unstressed open configuration at the beginning of the diastole, and the motion of the ventricular wall was neglected, the results obtained during the initial phases of opening are approximated. Analysis of the stress state of the MV has been performed when the valve is fully opened, when the effects of ventricular dynamics are reduced and the maximum principal stresses are constant. Previous analysis (Lau et al., 2010) of a single cardiac cycle (open–closed–open) has shown that during the second open period, when the valve is fully open, the maximum principal stresses are constant.

The biomechanical response of the functionally regurgitant valve was assumed to be identical to the normal valve. However, echocardiographic studies by Chaput et al. (2008) have shown that FMR results in increased MV leaflet area/volume, a change that will directly affect the biomechanical response of the valve. However, no data exists which has characterised the mechanical behaviour of MV tissue in this state.

The fluid volume has several simplifications regarding its geometry and dynamics of its boundaries. Here the ventricular chamber was designed as a rigid U-shaped volume with an open aortic position, factors which are all unphysiological. Also in functional regurgitant states the left ventricular volume is dilated, a factor ignored here as this model of dysfunction only includes valvular changes.

5. Conclusions

Here the functional response of the valve and fluid to a simulated dysfunctional state and subsequent surgical repair has been performed. Diastole was simulated using a FSI method with non-linear orthotropic material models used to described the mechanical response of the leaflets and chordae. Simulation of dysfunction has been performed by dilating the valve in the anteropostero axis to match the eccentricities reported *in vivo* in cases of functional MVR and subsequently corrected in two separate simulations: ETER with and without annuloplasty.

The results of the FSI simulations have shown that the maximum principal stresses induced in both corrected cases are 200% larger in a repaired valve compared to a normal valve. Although the maximum of both corrected scenarios are similar in magnitude, the distribution of the stress between the two cases differ significantly, with high stress concentrations in the dilated model with ETER only. Typically stresses in the MV in this portion of the cardiac cycle are low. Stress reduction will therefore be beneficial in minimising the detrimental effects of the ETER.

The fluid dynamics of filling are also affected, with highly directed flow generated by the ETER. Similar magnitudes of the velocity are observed downstream of the valve, however, the repaired valves exhibited diminished flow rates throughout the diastolic cycle, such that the peak flow rate was shifted from the end of the simulation to the start of diastole.

Conflict of interest

None.

Acknowledgements

K.D. Lau acknowledges the support of the BHF, ESPRC and MRC.

Appendix A. Supplementary data

Supplementary data associated with this article can be found in the online version at doi:10.1016/j.jbiomech.2011.06.030.

References

Alfieri, O., Bonis, M.D., 2010. The role of the edge-to-edge repair in the surgical treatment of mitral regurgitation. Journal of Cardiac Surgery 25 (5), 536–541.
Anyanwu, A.C., Bridgewater, B., Adams, D.H., 2010. The lottery of mitral valve repair surgery. Heart 96 (24), 1964–1967.
Avanzini, A., 2008. A computational procedure for prediction of structural effects of edge-to-edge repair on mitral valve. Journal of Biomechanical Engineering 130 (3), 031015.
Batchelor, G.K., 1967. An Introduction to Fluid Dynamics. Cambridge University Press.
Benson, D.J., 1992. Computational methods in Lagrangian and Eulerian hydrocodes. Computer Methods in Applied Mechanics and Engineering 99 (2–3), 235–394.
Burriesci, G., Howard, I.C., Patterson, E.A., 1999. Influence of anisotropy on the mechanical behaviour of bioprosthetic heart valves. Journal of Medical Engineering & Technology 23 (6), 203–215.
Chaput, M., Handschumacher, M.D., Tournoux, F., Hua, L., Guerrero, J.L., Vlahakes, G.J., Levine, R.A., 2008. Mitral leaflet adaptation to ventricular remodeling: occurrence and adequacy in patients with functional mitral regurgitation. Circulation 118 (8), 845–852.
Dal Pan, F., Donzella, G., Fucci, C., Schreiber, M., 2005. Structural effects of an innovative surgical technique to repair heart valve defects. Journal of Biomechanics 38 (12), 2460–2471.
Feldman, T., Kar, S., Rinaldi, M., Fail, P., Hermiller, J., Smalling, R., Whitlow, P.L., Gray, W., Low, R., Herrmann, H.C., Lim, S., Foster, E., Glower, D., 2009. EVEREST Investigators, 2009. Percutaneous mitral repair with the MitraClip system: safety and midterm durability in the initial EVEREST (endovascular valve edge-to-edge repair study) cohort. Journal of the American College of Cardiology 54 (8), 686–694.
Hallquist, J.O., 2006. LS-DYNA Theory Manual. Livermore Software Technology Corporation (LSTC).
Iung, B., Baron, G., Butchart, E.G., Delahaye, F., Gohlke-Bärwolf, C., Levang, O.W., Tornos, P., Vanoverschelde, J.L., Vermeer, F., Boersma, E., Ravaud, P., Vahanian, A., 2003. A prospective survey of patients with valvular heart disease in Europe: the euro heart survey on valvular heart disease. European Heart Journal 24 (13), 1231–1243.
Kaplan, S.R., Bashein, G., Sheehan, F.H., Legget, M.E., Munt, B., Li, X.N., Sivarajan, M., Bolson, E.L., Zeppa, M., Arch, M.Z., Martin, R.W., 2000. Three-dimensional echocardiographic assessment of annular shape changes in the normal and regurgitant mitral valve. American Heart Journal 139 (3), 378–387.
Kinnaird, T.D., Munt, B.I., Ignaszewski, A.P., Abel, J.G., Thompson, R.C., 2003. Edge-to-edge repair for functional mitral regurgitation: an echocardiographic study of the hemodynamic consequences. Journal of Heart Valve Disease 12 (3), 280–286.
Kunzelman, K.S., Cochran, R.P., 1990. Mechanical properties of basal and marginal mitral valve chordae tendineae. ASAIO Transactions 36 (3), M405–M408.
Kunzelman, K., Cochran, R., Chuong, C., Ring, W., Verrier, E., Eberhart, R., 1993. Finite element analysis of the mitral valve. Journal of Heart Valve Disease 2 (3), 326–340.
Kunzelman, K., Cochran, R., Verrier, E., Eberhart, R., 1994. Anatomic basis for mitral valve modelling. Journal of Heart Valve Disease 3 (5), 491–496.
Kunzelman, K., Einstein, D.R., Cochran, R.P., 2007. Fluid–structure interaction models of the mitral valve: function in normal and pathological states. Philosophical Transactions of the Royal Society B 362, 1393–1406.
Lam, J.H.C., Ranganathan, N., Wiglb, E.D., Silver, M.D., 1970. Morphology of the human mitral valve: I. Chordae Tendineae: a new classification. Circulation 41 (3), 449–458.
Lau, K.D., Diaz, V., Scambler, P., Burriesci, G., 2010. Mitral valve dynamics in structural and fluid–structure interaction models. Medical Engineering & Physics 32 (9), 1057–1064. doi:10.1016/j.medengphy.2010.07.008.
Levick, J., 2003. An Introduction to Cardiovascular Physiology, fourth ed.
LS-DYNA Keyword User's Manual, 2007. Livermore Software Technology Corporation (LSTC), 971 ed.
Maisano, F., Caldarola, A., Blasio, A., Bonis, M.D., Canna, G.L., Alfieri, O., 2003. Midterm results of edge-to-edge mitral valve repair without annuloplasty. Journal of Thoracic and Cardiovascular Surgery 126 (6), 1987–1997.
May-Newman, K., Yin, F.C., 1995. Biaxial mechanical behavior of excised porcine mitral valve leaflets. American Journal of Physiology 269 (4 Pt 2), H1319–H1327.
Redaelli, A., Guadagni, G., Fumero, R., Maisano, F., Alfieri, O., 2001. A computational study of the hemodynamics after 'edge-to-edge' mitral valve repair. Journal of Biomechanical Engineering 123 (6), 565–570.
Sakai, T., Okita, Y., Ueda, Y., Tahata, T., Ogino, H., Matsuyama, K., Miki, S., 1999. Distance between mitral annulus and papillary muscles: anatomic study in normal human hearts. Journal of Thoracic and Cardiovascular Surgery 118, 636–641.

Salgo, I.S., Gorman, I., Joseph, H., Gorman, R.C., Jackson, B.M., Bowen, F.W., Plappert, T., St John Sutton, M.G., Edmunds, J., Henry, L., 2002. Effect of annular shape on leaflet curvature in reducing mitral leaflet stress. Circulation 106 (6), 711–717.
Verma, S., Mesana, T.G., 2009. Mitral-valve repair for mitral-valve prolapse. New England Journal of Medicine 361 (23), 2261–2269.
Veronesi, F., Corsi, C., Sugeng, L., Mor-Avi, V., Caiani, E.G., Weinert, L., Lamberti, C., Lang, R.M., 2009. A study of functional anatomy of aortic-mitral valve coupling using 3D matrix transesophageal echocardiography. Circulation: Cardiovascular Imaging 2 (1), 24–31.
Votta, E., Maisano, F., Soncini, M., Redaelli, A., Montevecchi, F.M., Alfieri, O., 2002. 3-D computational analysis of the stress distribution on the leaflets after edge-to-edge repair of mitral regurgitation. Journal of Heart Valve Disease 11 (6), 810–822.
Votta, E., Caiani, E., Veronesi, F., Soncini, M., Montevecchi, F.M., Redaelli, A., 2008. Mitral valve finite-element modelling from ultrasound data: a pilot study for a new approach to understand mitral function and clinical scenarios. Philosophical Transactions of the Royal Society A: Mathematical, Physical and Engineering Sciences 366 (1879), 3411–3434.